# Electrical spin injection in metallic mesoscopic spin valves

Jedema, Friso

# Chapter 5

# Spin injection in F/N/F systems with transparent contacts

## 5.1 Introduction

The electrical injection and detection of spin accumulation is studied in lateral ferromagnetic metal-nonmagnetic metal-ferromagnetic metal (F/N/F) spin valve devices with transparent interfaces. Different ferromagnetic metals, permalloy (Py), cobalt (Co) and nickel (Ni), are used as electrical spin injectors and detectors. For the nonmagnetic metal both aluminium (Al) and copper (Cu) are used. The magnetoresistance of the ferromagnetic contacts is found to be able to dominate the amplitude of the spin valve effect, making it impossible to observe the spin valve effect in a 'conventional' measurement geometry. However, in a 'non local' spin valve measurement it is possible to completely isolate the spin valve signal and observe clear spin accumulation signals at $T =$ 4.2 K as well as at room temperature (RT). For Al spin relaxation lengths ($\lambda_{sf}$) are obtained of 1.2 $\mu$m and 600 nm at $T = 4.2$ K and RT respectively, whereas for Cu 1.0 $\mu$m and 350 nm found. At RT these spin relaxation lengths are within a factor 2 of their maximum values, being limited by phonon mediated spin flip processes. The spin valve signals generated by the Py electrodes ($\alpha_F \lambda_F = 0.5$ [1.2] nm at RT [$T = 4.2$ K]) are found to be larger than the Co electrodes ($\alpha_F \lambda_F = 0.3$ [0.7] nm at RT [$T = 4.2$ K]), whereas for Ni ($\alpha_F \lambda_F < 0.3$ nm at RT and $T = 4.2$ K) no spin signal could be observed.

## 5.2 Spin accumulation in Py/Cu/Py spin valves

Permalloy $Ni_{80}Fe_{20}$ (Py) ferromagnetic electrodes are used to drive a spin polarized current into copper (Cu) crossed strips. For fabrication details and

properties, see Chapter 3. Different aspect ratios of the rectangular ferromagnetic injector (Py1) and detector strips (Py2) result in different switching fields of the magnetization reversal process, allowing control over the relative magnetization configuration of Py1 and Py2 (parallel/anti-parallel) by applying a magnetic field parallel to the long axis of the ferromagnetic electrodes [1, 2], see Chapter 4. Two sets [Py1,Py2] of different sizes are used in the experiments. One set has dimensions of $2 \times 0.8\ \mu m^2$ (F1) and $14 \times 0.5\ \mu m^2$ (F2), whereas the other set has dimensions of $2 \times 0.5\ \mu m^2$ (F1) and $14 \times 0.15\ \mu m^2$ (F2). An example of a typical device is shown in Fig. 3.6.

The measurements were performed by standard ac-lock-in-techniques, using current magnitudes of 100 $\mu A$ to 1 mA. Typical spin valve signals of two samples MSV1 and MSV2 (of the same batch) with a Py electrode spacing of $L =$ 250 nm are shown in the Figs. 5.1, 5.2 and 5.3. They are both measured in a non local and conventional measurement geometry. Sample MSV1, data shown in Fig. 5.1 and 5.2, had a current injector Py1 electrode of size $2 \times 0.5\ \mu m^2$, whereas the detector electrode Py2 had a size of $14 \times 0.15\ \mu m^2$. Sample MSV2, data in shown Fig. 5.3, had wider Py electrodes of $2 \times 0.8\ \mu m^2$ and $14 \times 0.5\ \mu m^2$. The first set of (narrower) Py electrodes [Py1,Py2] had a more ideal switching behavior and had three times larger switching fields as compared to the second set [Py1,Py2], see also Chapter 4.

### 5.2.1 Non local spin valve geometry

Figure 5.1a and 5.1b show typical data in the non local measurement geometry taken at 4.2 K and RT for sample MSV1 with a 250 nm Py electrode spacing. Sweeping the magnetic field from negative to positive field, an increase in the resistance is observed, when the magnetization of Py1 flips at 9 mT, resulting in an anti-parallel magnetization configuration. The rise in resistance is due to the spin accumulation or equivalently an excess spin density present in the Cu metal. When the magnetization of Py2 flips at 47 mT ($T = 4.2$ K) and 38 mT (RT), the magnetizations are parallel again, but now point in the opposite direction. The magnitude of the measured background resistance, around 30 $m\Omega$ at $T = 4.2$ K and 120 $m\Omega$ at RT, depends on the geometrical shape of the Cu cross and is typically a fraction of the Cu square resistance.

Figure 5.1c and 5.1d show the "memory effect". Coming from high positive B field, the sweep direction of the B field is reversed after Py1 has switched, but Py2 has not. At the moment of reversing the sweep direction, the magnetic configuration of Py1 and Py2 is anti-parallel, and accordingly a higher resistance is measured. When the B-field is swept back to its original high positive value, the resistance remains at its increased level

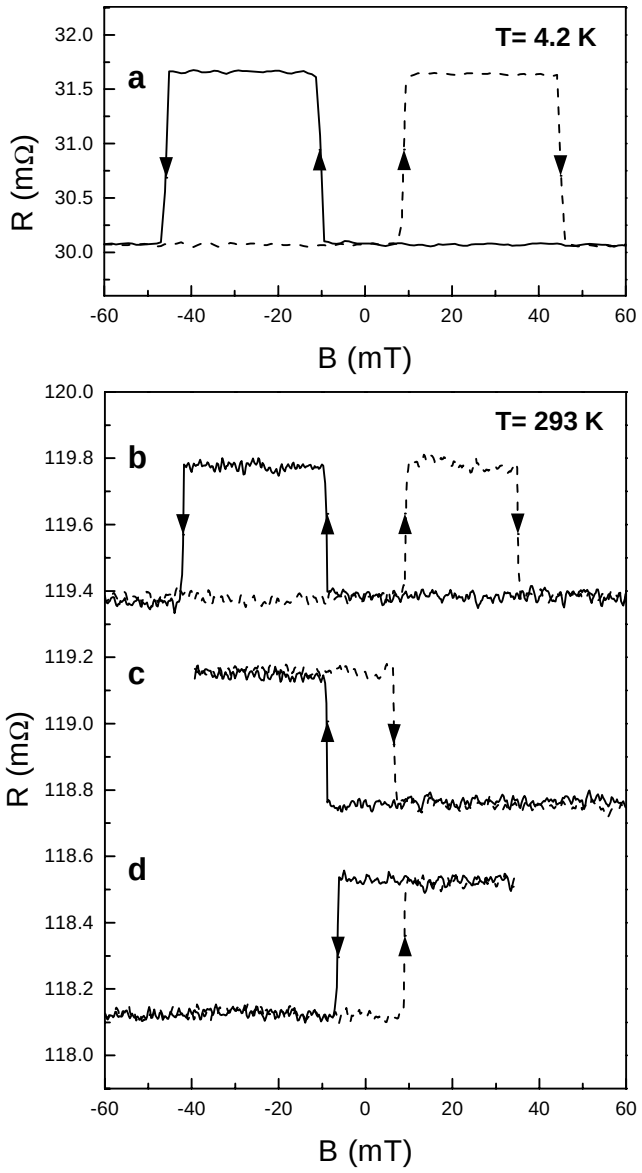


Figure 5.1: *The spin valve effect at $T = 4.2$ K (a) and RT (b) in the non-local geometry for a Py/Cu/Py spin valve device (sample MSV1) with 250 nm Py electrode spacing. An increase in resistance is observed, when the magnetization configuration is changed from parallel to anti-parallel. The solid (dashed) lines correspond to the negative (positive) sweep direction. (c),(d) illustrate the "memory effect". For clarity the (c) and (d) are off set downwards. Note that the vertical scale of (a) is different from (b),(c) and (d). The sizes of the Py1 and Py2 electrodes are $2 \times 0.5$ $\mu m^2$ and $14 \times 0.15$ $\mu m^2$*

until Py1 switches back at a positive field of 9 mT. At zero B field the resistance can therefore have two distinct values, depending on the history

of the Py electrodes.

### 5.2.2 Conventional spin valve geometry

The top curve in Fig. 5.2 shows the magnetoresistance behavior of sample MSV1 in the conventional measurement geometry. A small AMR contribution (dip in curve) of the Py1 electrode around $-9$ mT and a small Hall signal caused by the Py2 electrode can be observed in the negative sweep direction. Because a small part of the Py electrodes underneath the Cu wire is measured in this geometry, (local) changes in the magnetization at the Py/Cu contact area can produce an AMR or Hall signal [3]. In the positive sweep direction a dip is no longer observed indicating that the magnetization reversal of the Py1 electrode is not the same for the two sweep directions. However, in the magnetic field range in between the two switching fields, a resistance 'plateau' from 10 mT up to a field of 45 mT is observed.

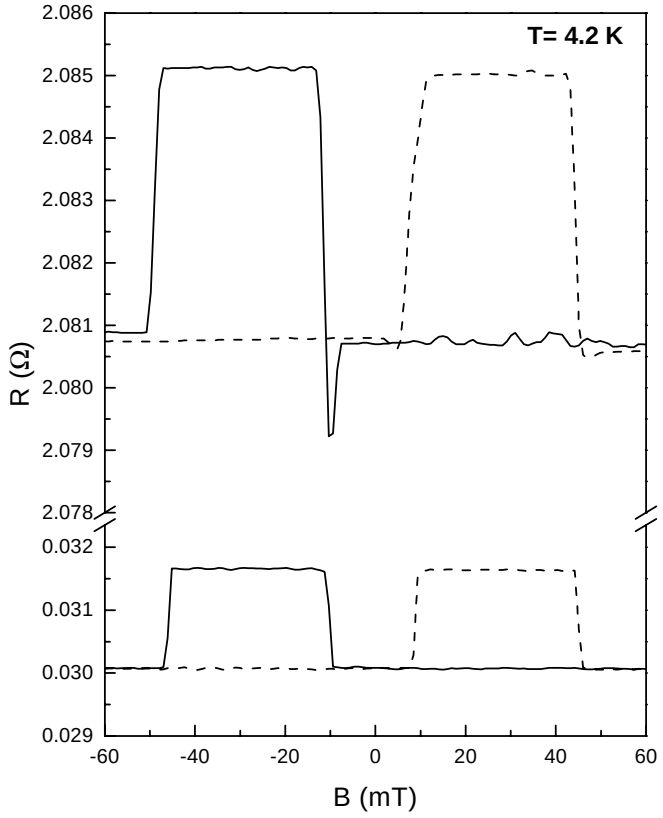


Figure 5.2: *The spin valve effect of sample MSV1 in a conventional measurement geometry (top curve) at $T = 4.2$ K and non-local measurement geometry (bottom curve), with a Py electrode spacing $L = 250$ nm. The sizes of the Py electrodes are $2 \times 0.5$ $\mu m^2$ (Py1) and $14 \times 0.15$ $\mu m^2$ (Py2). The solid (dotted) curve corresponds with a negative (positive) sweep direction of the B-field.*

The magnitude of the spin valve effect measured in the conventional geometry is about 4.1 $m\Omega$ at $T = 4.2$. This is about 2.5 times bigger than the magnitude of the spin signal measured in a non-local geometry (1.6 $m\Omega$). Note that the factor 2.5 is deviating from the factor 2 as predicted by the Eq. 2.36. This is attributed to deviations from our 1-dimensional model, which can be expected for the samples with the shortest Py electrode spacing $L = 250$ nm, as the presence of the Cu side arms for these samples, see Fig. 3.6, are most felt.

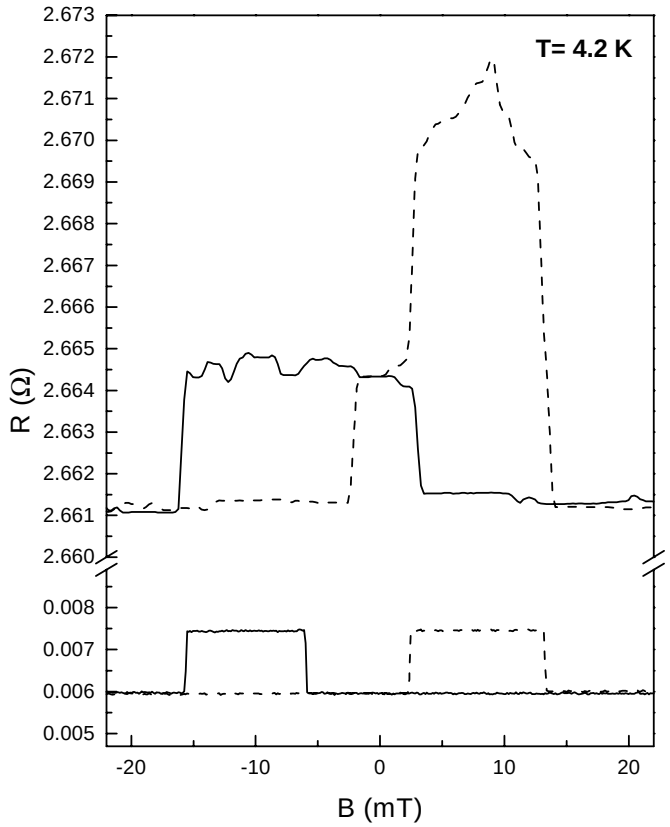


Figure 5.3: *The spin valve effect of sample MSV2 in a conventional measurement geometry (top curve) at $T = 4.2$ K and non-local measurement geometry (bottom curve), with a Py electrode spacing $L = 250$ nm. The sizes of the Py electrodes are $2 \times 0.8$ $\mu m^2$ (Py1) and $14 \times 0.5$ $\mu m^2$ (Py2). The solid(dotted) curve corresponds with a negative (positive) sweep direction of the B-field.*

The top curve in Fig. 5.3 shows the magnetoresistance behavior in the conventional measurement geometry for the sample MSV2. Here a change of the resistance is already observed before the field has reached zero in a positive field sweep, whereas the negative field sweep is very asymmetrical compared to the positive field sweep. This is attributed to the formation of a multi-domain structure in the $2 \times 0.8$ $\mu m^2$ (Py1) electrode, causing a large

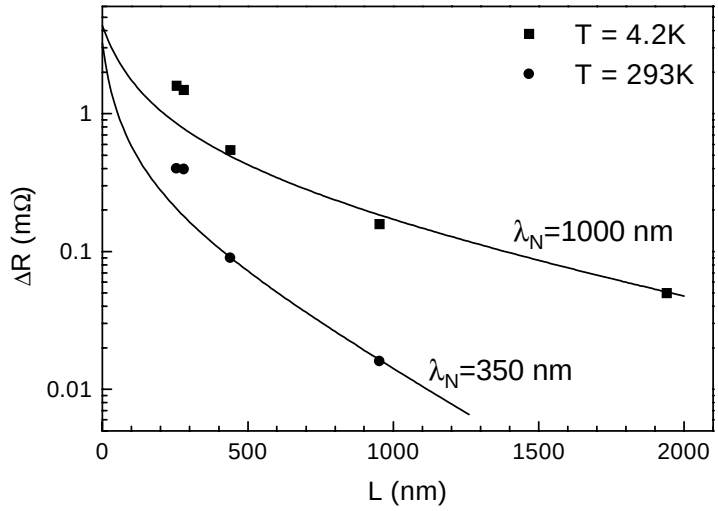


Figure 5.4: *Dependence of the magnitude of the spin signal $\Delta R$ on the Py electrode distance L, measured on Py/Cu/Py samples in the non local geometry. The solid squares represent data taken at $T =$ 4.2 K, the solid circles represent data taken at RT. The solid lines represent the best fits based on equation 2.31.*

AMR ($\approx 10\ m\Omega$) signal at the Py/Cu contact area of the Py1 electrode (see also Chapter 4).

However, in a non local measurement geometry, the "contact" magnetoresistance contribution of the Py electrodes can be removed and a clear spin valve signal is observed with a similar magnitude as sample MSV1. This is shown in the bottom curve of Fig. 5.3. Note also that the larger widths and aspect ratio of the Py electrodes in sample MSV2 result in three times smaller switching fields as compared to sample MSV1.

### 5.2.3 Dependence on Py electrode spacing

A reduction of the magnitude of spin signal $\Delta R$ is observed with increased electrode spacing $L$ , as shown in Fig. 5.4. By fitting the data to Eq. 2.31 the spin relaxation length $\lambda_N$ in the Cu wire is obtained. From the best fits a value of 1 $\mu m$ at $T =$ 4.2 K, and 350 nm at RT is found. These values are compatible with those reported in literature, where 450 nm is obtained for Cu in GMR measurements at 4.2 K [4]. However a detailed discussion on the obtained spin relaxation lengths and corresponding spin relaxation times will be given in §5.5.

In principle the fits of Fig. 5.4 also yield the spin polarization $\alpha_F$ and the spin relaxation length $\lambda_F$ of the Py electrodes. However, the values of $\alpha_F$ and $\lambda_F$ cannot be determined separately, as in the relevant limit ($M >> 1$) which applies to the Py/Cu/Py experiments ($12 < M < 26$),

the spin signal $\Delta R$ is proportional to the product $\alpha_F \lambda_F$ as is shown by Eq. 2.33. From the best fits the value $\alpha_F \lambda_F$ is obtained: $\alpha_F \lambda_F =$ 1.2 nm at 4.2 K and $\alpha_F \lambda_F =$ 0.5 nm at RT. Taking, from literature [5–7], a spin relaxation length in the Py electrode of $\lambda_F =$ 5 nm (at 4.2 K), a bulk current polarization of $\approx 20$ % in the Py electrodes at $T =$ 4.2 K is obtained: $\alpha_F =$ 0.2. Note however that the injected spin polarized current from the Py electrode is partially shunted by the Cu wire lying on top of the Py electrode. By taking this effect into account the value $\alpha_F \lambda_F$ could be increased by a factor 2 to 3.

It is also possible to calculate the polarization of the current at the Py/Cu interface. For a sample with a Py electrode spacing of $L = 250$ nm at $T = 4.2$ K and using Eq. 2.34 we find: $P \simeq 0.02$, a factor 10 lower than the bulk polarization $\alpha_F$ of the Py electrodes. From the resistor model one can see why the current polarization at the Py/Cu interface is reduced. For this, first a calculation of the magnitude of the spin dependent resistance difference is needed. Using Eq. 2.42 and $L = 250$ nm, $\Delta R = 1.6\ m\Omega$, $R^N_\Box = 0.3\ \Omega$ and $w = 100$ nm ( at $T = 4.2$ K) a value of $R_\downarrow - R_\uparrow \approx 100\ m\Omega$ is found. From the right hand side term of Eq. 2.42 and using $R^F_\Box = 2\ \Omega$ it can be checked that this indeed corresponds with the value of $\alpha_F \lambda_F \approx$ 1.2 nm, as was also obtained from the fit in Fig. 5.4. From Eqs. 2.37, 2.38 and using $\lambda_F =$ 5 nm, $\alpha_F =$ 0.2 (at 4.2 K) the spin-up and spin-down resistance of the Py ferromagnet can be obtained:

$$R^{Py}_\uparrow = \frac{2\lambda_F}{w(1+\alpha_F)} R^F_\Box \approx 160\ m\Omega \tag{5.1}$$

$$R^{Py}_\downarrow = \frac{2\lambda_F}{w(1-\alpha_F)} R^F_\Box \approx 260\ m\Omega\ . \tag{5.2}$$

This shows that the total resistance experienced over a length $\lambda_F + \lambda_N$ by the spin-up and spin-down currents is indeed dominated by the spin *independent* resistance $2R^N = 2\lambda_N R^N_\Box / w \simeq 6\ \Omega$. Here the values of $\lambda_N = 1\ \mu m$, $R^N_\Box = 0.3\ \Omega$ at $T = 4.2$ K and $w = 100$ nm are used. This leads to a interface polarization of $P \approx (R_\downarrow - R_\uparrow)/(R_\uparrow + R_\downarrow + 4R^N) \approx 1$ % at the Py/Cu interface.

All though the role of an interface resistance $R_{int}$ for spin injection will be described in the next paragraph, it is noted here that the small difference $R_\downarrow - R_\uparrow \approx 100\ m\Omega$ responsible for a spin valve signal of $\Delta R = 1.6\ m\Omega$ could possibly also result from an interface resistance at the Py/Cu interface. Commonly reported resistivities of $5 \cdot 10^{-16}\ \Omega m^2$ for the Py/Cu interface [5–9] and a contact area of $S = 1 \cdot 10^{-14}\ m^2$ (i.e. $R_{int} = 50\ m\Omega$) would yield a realistic interface polarization of $\gamma = 0.5$ for the Py/Cu interface, using Eq. 5.3. However, the specific details of the spin injection mechanism

(interface, bulk or a combination) do not alter the conclusion that the total spin dependent resistance $R_\downarrow - R_\uparrow \approx 100\ m\Omega$ is dominated by the spin independent resistance of the Cu strip over a spin relaxation length and hence leads to a considerable reduction of the spin valve signal, as was pointed out above.

### 5.2.4 Comparison with Johnson Spin Transistor

The magnitude of the spin signals in the Py/Cu/Py samples, when scaled to the cross sections utilized in the Au thin film devices of Ref. [10–12] (the "Johnson spin transistor"), are more than $10^4$ times smaller than obtained in that previous work. However, in that earlier work it was necessary to invoke a spin polarization exceeding 100 % to explain the results in terms of spin accumulation [10–12]. This contrasts our results, which yield a spin polarization P of the current at the Py/Cu interface of about $1 - 2\%$.

In Refs. [10–13] and [14] Johnson postulates that spin injection is mediated by interfacial transport, because the interface resistances $R_\uparrow^{int}$, $R_\downarrow^{int}$ would dominate the total resistance in both spin-up and spin-down channels: $R_\uparrow^{int} > R_\uparrow^F + 2R^N$ and $R_\downarrow^{int} > R_\downarrow^F + 2R^N$ respectively. Here $R_\uparrow^F$ and $R_\downarrow^F$ are defined as in Eqs. 2.37 and 2.38 and $R^N = \lambda_N/\sigma_N S = \lambda_N R_\square^N/w$. In this limit spin injection would be characterized by the interfacial spin injection parameter defined as:

$$\eta = \frac{R_\downarrow^{int} - R_\uparrow^{int}}{R_\uparrow^{int} + R_\downarrow^{int}} \ , \tag{5.3}$$

and Johnson derives the following expression (see also Eq. 2.57) for the spin accumulation signal in a nonmagnetic region N of volume $V = S \cdot L$ [12, 13]:

$$\Delta R = \frac{2\eta^2 \lambda_N^2}{\sigma_N S L} \ . \tag{5.4}$$

Applying Eq. 5.4 in Ref. [13] Johnson calculates an expected spin signal of $\Delta R = 1.9\ \Omega$ for our device with the shortest Py electrode spacing $L = 250$ nm, as calculated by using $S = 5{\cdot}10^{-15}\ m^2$, $\sigma_{Cu} = 7.1{\cdot}10^7\ \Omega^{-1}m^{-1}$, $\eta = 0.4$ and $\lambda_N = 1.0\ \mu m$.

However a polarization of the current at the Py/Cu interface of $\eta = 40$ % would require spin dependent interface resistances of $R_\uparrow^{int} = 16\ \Omega$ and $R_\downarrow^{int} = 37\ \Omega$, using Eqs. 5.3, 2.40 and replacing Eqs. 2.37 and 2.38 by:

$$R_\uparrow \ = \ R_\uparrow^{int} + R_\uparrow^F + R^{SD} \ , \tag{5.5}$$

$$R_{\downarrow} \;=\; R_{\downarrow}^{int} + R_{\downarrow}^{F} + R^{SD} \;, \tag{5.6}$$

where the spin dependent interface resistances $R_{\uparrow}^{int}$ and $R_{\downarrow}^{int}$ have simply been added up to bulk spin dependent resistances $R_{\uparrow}^{F}$ and $R_{\downarrow}^{F}$ because the spin polarization $\eta$ as well as the bulk spin polarization $\alpha_F$ are found to be positive ($\alpha_F > 0$ and $\eta > 0$) for Py and Cu [5–7, 15]. The values $R_{\uparrow}^{int} = 16\ \Omega$ and $R_{\downarrow}^{int} = 37\ \Omega$ yield a total single interface resistance $R_{int} = 11\ \Omega$ or equivalently, a interface resistivity of $1 \cdot 10^{-13}\ \Omega m^2$. This is more than a 100 times larger then the upper limit 0.1 $\Omega$ or equivalently a contact resistivity of $1 \cdot 10^{-15}\ \Omega m^2$ that could be determined from our experiment, see Figs. 5.2 and 5.3.

The above arguments also apply for the experiment of Refs. [10–12] where a gold layer is sandwiched in between two Py layers. There is no physical reason why there should exist an interface resistivity larger than $1 \cdot 10^{-13}\ \Omega m^2$ between the Au and Py or Co layers in the experiment of Ref. [10, 11], which can explain an interface current polarization of $\eta = 0.4$ or more. Equation 5.4 can therefore not be applied to the experiment of Ref. [10, 11], because it does not include the (fast) spin relaxation reservoirs of the ferromagnetic injector and detector contacts, which dominate the total spin relaxation in the case of transparent contacts, as was already pointed out in Refs. [16, 17].

In view of this, given the unexplained discrepancies ($\eta > 3$) of the earlier work in Ref. [10–12], and the more consistent values obtained in the recent work, it is the author's opinion that the results of Refs. [10–12] cannot be reconciled with spin injection and spin accumulation.

## 5.3 Spin accumulation in Py/Al/Py spin valves

Here spin injection experiments are described using permalloy $Ni_{80}Fe_{20}$ (Py) strips as ferromagnetic electrodes to drive a spin polarized current via transparent contacts into aluminum (Al) crossed strips, see Fig. 3.6. Similar current polarizations and spin relaxation lengths for Py and Al are obtained as in Section 5.2.

### 5.3.1 Spin valve measurements

Figure 5.5 shows a typical spin valve signal of a Py/Al/Py sample with a Py separation spacing of $L = 250$ nm and Py electrodes of sizes $2 \times 0.8\ \mu m^2$ and $14 \times 0.5\ \mu m^2$.

The top curve in Fig. 5.5 shows the magnetoresistance behavior in the conventional measurement geometry. Again the magnetoresistance signals

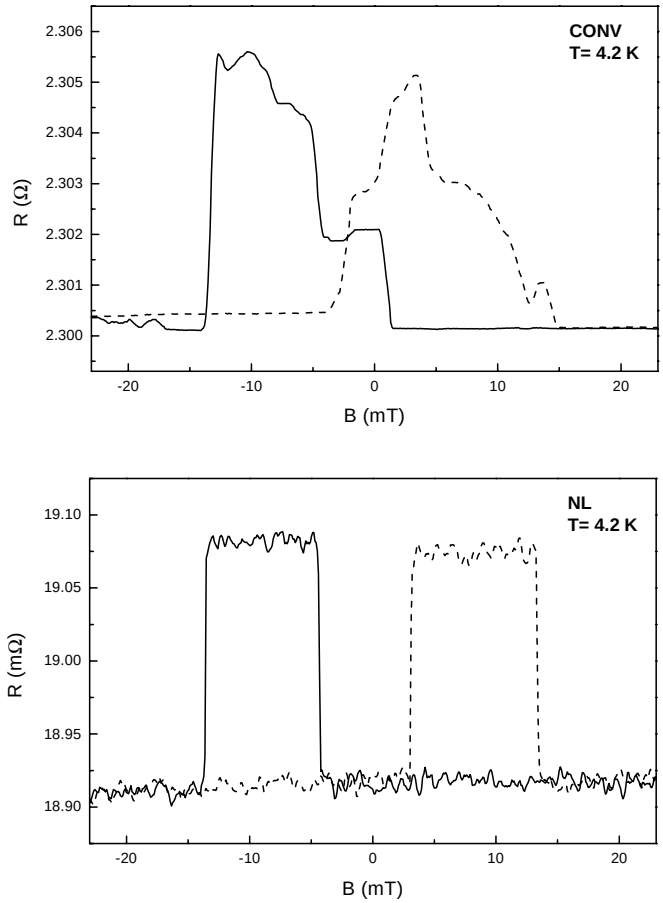


Figure 5.5: *The spin valve effect of a Py/Al/Py sample using a conventional measurement geometry (CONV, top curve) at $T = 4.2$ K and non-local measurement geometry (NL, bottom curve), with a Py electrode spacing $L = 250$ nm. The sizes of the Py electrodes are $2 \times 0.8$ $\mu m^2$ (Py1) and $14 \times 0.5$ $\mu m^2$ (Py2). The solid (dotted) curve corresponds with a negative (positive) sweep direction of the B-field.*

of the Py contacts are dominating in this geometry, reaching a maximal amplitude of about 6 $m\Omega$. Note that the two resistance values at high positive and negative field differ by a value of about 0.3 $m\Omega$, which is attributed to a local hall effect caused by the $14 \times 0.5$ $\mu m^2$ Py electrode. The bottom curves in Fig. 5.5 show magnetic field sweeps in the non local measurement geometry, which clearly shows a spin valve signal having removed all spurious contact magnetoresistance effects. The magnitude of the spin valve signal measured is 0.18 $m\Omega$ at 4.2 K.

### 5.3.2 Dependence on Py electrode spacing

A reduction of the magnitude of spin signal $\Delta R$ of the Py/Al/Py samples is observed with increased electrode spacing $L$, as shown in Fig. 5.6. However, for the $T = 4.2$ K data this dependence is not monotonic. The spin valve devices with small $L = 250$ nm and $L = 500$ nm show a smaller spin valve signal than the device with $L = 1\ \mu m$. We note that all the devices shown in Fig. 5.6 are from the same (processing) batch. However, the granular structure of the Al film with a grain size in the order of the width of the Al strip causes fluctuations in the resistance of the Al strip in between the Py electrodes. The samples with $L = 250$ nm and $L = 500$ nm indeed show a higher resistance than expected when measured in the conventional geometry at $T = 4.2$ K. This irregular behavior of the resistance due to grains is not observed at RT due to the additional presence of phonon scattering. From the best fits to Eq. 2.31 a spin relaxation length $\lambda_N$ in Al of 1.2 $\mu m$ at $T =$ 4.2 K and 600 nm at RT is found. Note that the spin relaxation lengths are about 2 times larger than reported in Ref. [18]. The reason for this increase is the higher conductivity of the Al in these samples, caused by a lower background pressure of $1 \cdot 10^{-8}$ mbar during evaporation as compared to a background pressure of $1 \cdot 10^{-6}$ mbar used in Ref. [18].

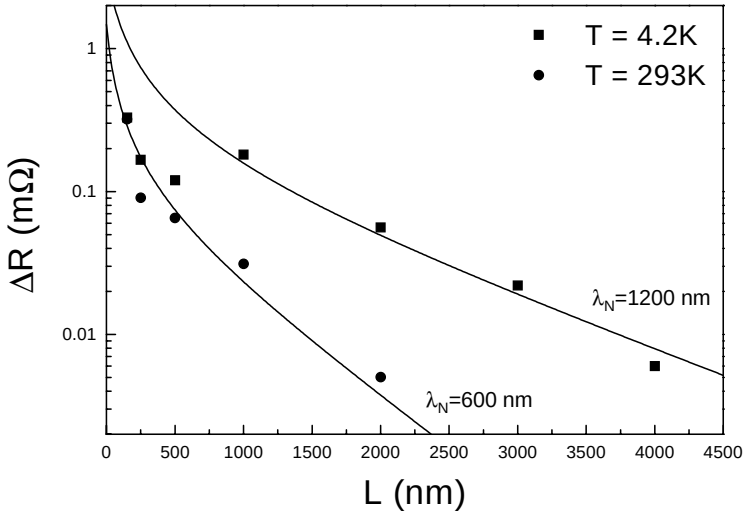


Figure 5.6: *Dependence of the magnitude of the spin signal $\Delta R$ on the Py electrode distance L, measured in the non local geometry for Py/Al/Py spin valves. The solid squares represent data taken at $T =$ 4.2 K, the solid circles represent data taken at RT. The solid lines represent the best fits based on Eq. 2.31.*

The fits of Fig. 5.6 also yield the spin polarization $\alpha_F$ and the spin relaxation length $\lambda_F$ of the Py electrodes. Their values are found to be $\alpha_F \lambda_F =$ 1.2 nm at 4.2 K and $\alpha_F \lambda_F =$ 0.5 nm at RT, in agreement with

the Py/Cu/Py spin valve data of Sec. 5.2. Note that for the Py/Al/Py spin valve also applies that $M >> 1$ and thus the spin signal $\Delta R$ is proportional to the product $\alpha_F \lambda_F$ ($25 < M < 32$). Using Eq. 2.34, a polarization P for the Py/Al/Py sample with the smallest Py electrode spacing of $L =$ 250 nm at $T = 4.2$ K is found to be only 3%: $P = 0.03$.

## 5.4 Spin injection using Co and Ni ferromagnetic electrodes

From Eq. 2.42 it can be seen that the magnitude of the spin dependent resistance $(R_\downarrow - R_\uparrow)$ is sensitive to the properties $\alpha_F$, $\lambda_F$ and $\sigma_F$ of the ferromagnetic metal. As $(R_\downarrow - R_\uparrow)$ enters squared in the spin valve signal $\Delta R$, see Eq. 2.40, an increase of $\lambda_F$ with a factor 10 would increase $\Delta R$ with a factor 100. Therefore cobalt (Co) and nickel (Ni) are tried as ferromagnetic spin injectors and detectors to increase the magnitude of the spin valve signal, as larger spin relaxation lengths can be expected for these materials [19–21].

### 5.4.1 Spin accumulation in Co/Cu/Co spin valves

Figure 5.7a shows a "contact" magnetoresistance trace and magnetic switching behavior at RT of a $14 \times 0.5$ $\mu m^2$ (Co2) electrode of a Co/Cu/Co spin valve device with a Co electrode spacing of 250 nm and Co electrodes of sizes $2 \times 0.8$ $\mu m^2$ and $14 \times 0.5$ $\mu m^2$. The "contact" magnetoresistance is measured by sending current from contact 5 to 7 and measuring the voltage between contacts 6 and 9 (see Fig. 3.7d). Note that in this geometry the measured voltage is not sensitive to a spin valve signal as only one Co electrode is used in the measurement configuration. The magnetoresistance traces of Fig. 5.7a indicate a clear switching of the magnetization at $\pm 20$ mT of the $14 \times 0.5$ $\mu m^2$ Co2 electrode and is attributed to a local Hall effect produced at the Co/Cu contact area of the Co2 electrode.

Figure 5.7b shows the spin valve effect at RT for a Co/Cu/Co spin valve device in a non local measurement. The magnitude of the spin dependent resistance $\Delta R = 0.25$ $m\Omega$ is slightly smaller than in the Py/Cu/Py spin valve device. At $T = 4.2$ K the signal increases to $\Delta R = 0.8$ $m\Omega$. Using Eq. 2.31 and the values of $\sigma_N$, $\lambda_N$ for Cu and $\sigma_F$ for Co (see Chapter 3), values of $\alpha_F \lambda_F = 0.3$ nm at RT and $\alpha_F \lambda_F = 0.7$ nm at $T = 4.2$ K are obtained. These values are much smaller than reported for Co in GMR experiments, where $\alpha_F \approx 0.5$ and $\lambda_F = 10 - 60$ nm [5, 22–26]. This discrepancy will be discussed in Section 5.5.2.

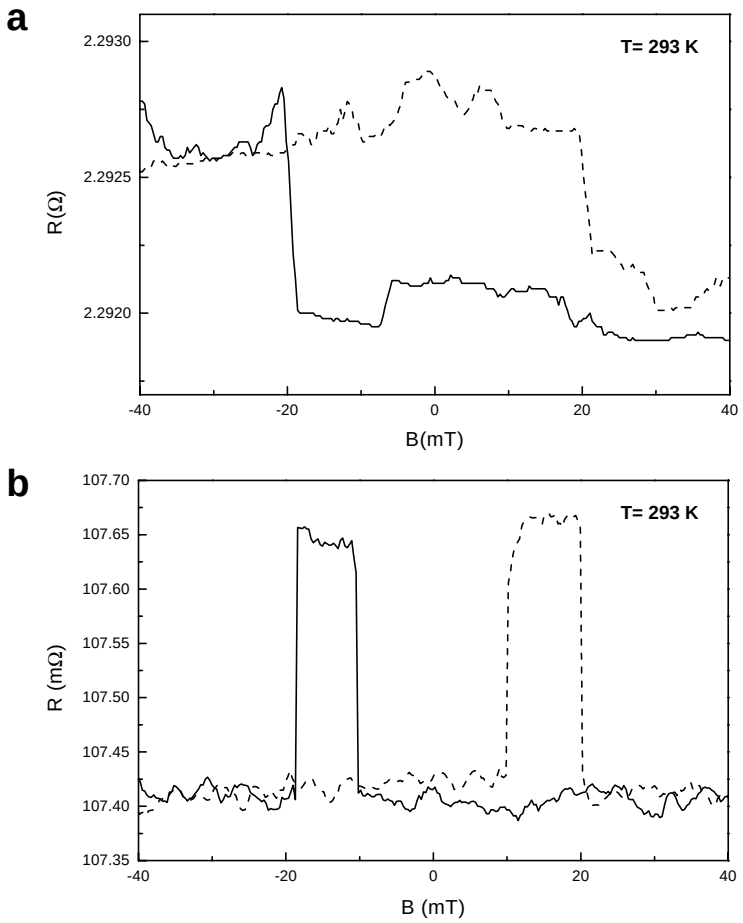


Figure 5.7: *a, "Contact" magnetoresistance trace of the Co2 electrode with size* $14 \times 0.5\ \mu m^2$*. The Hall signal indicates an abrupt magnetization switching of the Co2 electrode. b, The spin valve effect at RT in a Co/Cu/Co device with a Co electrode spacing* $L = 250$ *nm, using the non local measurement geometry. The solid (dotted) curve corresponds with a negative (positive) sweep direction of the B-field.*

### 5.4.2 Spin accumulation in Ni/Cu/Ni spin valves

In Fig. 5.8a and 5.8b two "contact" magnetoresistance traces of a Ni electrode (Ni1) with size $2 \times 0.5\ \mu m^2$ (top curve) and a Ni electrode (Ni2) with size $14 \times 0.15\ \mu m^2$ (middle curve) are shown of a Ni/Cu/Ni spin valve device with a Ni electrode spacing of 500 nm. For the Ni1 contact current is send from contact 1 to 5 and the voltage is measured from contact 4 to 6 (see Fig. 3.7c). For the Ni2 contact current is send from contact 5 to 7 and the voltage is measured from contact 6 to 9 (see Fig. 3.7d). The magnetic field in the measurements of Fig. 5.8 is applied perpendicular to the long axis of the Ni electrodes, showing a more pronounced magnetic switching

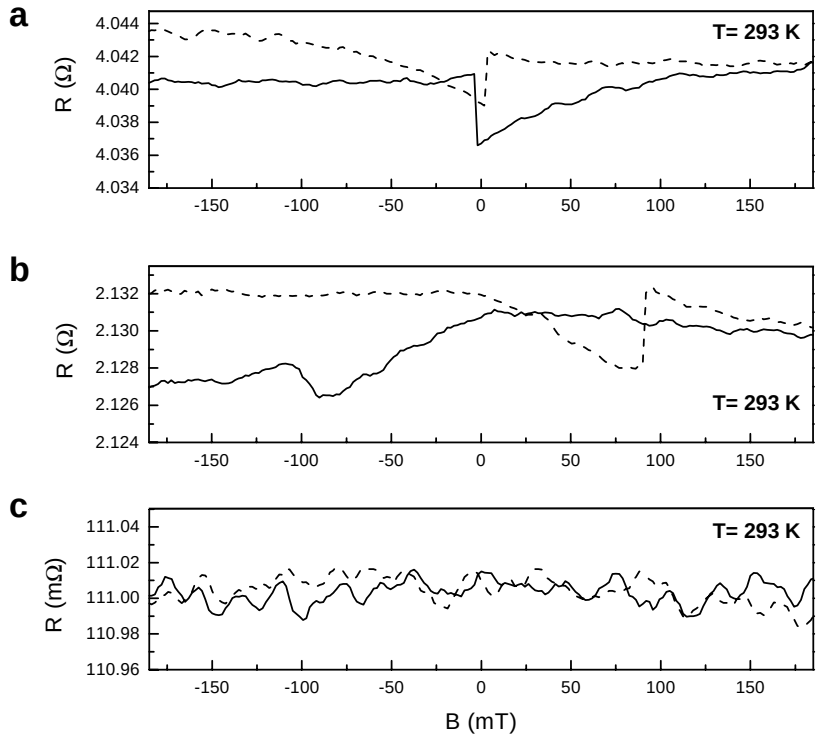


Figure 5.8: *(a) "Contact" magnetoresistance trace (see text) of the Ni1 electrode with size* $2 \times 0.5\ \mu m^2$. *(b) "Contact" magnetoresistance trace of the Ni2 electrode with size* $14 \times 0.15\ \mu m^2$. *(c) The spin valve effect of a Ni/Cu/Ni device at RT with a Ni electrode spacing of* $L = 500$ *nm, using a non local measurement geometry. The solid (dotted) curve corresponds with a negative (positive) sweep direction of the B-field.*

behavior than an applied magnetic field along the long axis of the Ni electrodes. In the magnetic field sweeps of Figs. 5.8a and 5.8b a large magnetic field range can be observed where the magnetization configuration of the Ni electrodes is anti-parallel. However no spin valve signal could be detected within experimental accuracy in the non local measurement geometry at RT as well as at $T = 4.2$ K, as is shown in Fig. 5.8c (RT). An upper bound on the spin valve signal is found to be $\Delta R < 20\ \mu\Omega$ at RT as well as at $T = 4.2K$. Using Eq. 2.31 and the values of $\sigma_N$, $\lambda_N$ for Cu and $\sigma_F$ for Ni (see Chapter 3), values of $\alpha_F \lambda_F < 0.3$ nm at RT as well as at $T = 4.2$ K are obtained. These values are also much smaller than reported for Ni in GMR experiments, where $\alpha_F \approx 0.2$ [15, 27] and using a calculated $\lambda_F = 15$ nm. The calculation of $\lambda_F$ for Ni and the low value of $\alpha_F \lambda_F < 0.3$ nm is discussed next in Section 5.5.2.

## 5.5 Spin relaxation times of conduction electrons in metals

In this section our obtained spin relaxation lengths ($\lambda_{sf}$) and their associated spin relaxation times ($\tau_{sf}$) in Cu and Al from the spin injection experiments in sections 5.2, 5.3, 5.4 and Chapter 6 will be analyzed and compared with theory and previously reported values from CPP-GMR [28], CESR [29], weak localization [30] and superconducting tunneling experiments [31]. The obtained spin polarization and spin relaxation lengths in Py, Co and Ni will be compared with reported values from CPP-GMR experiments.

In CESR experiments the measured electron spin transverse relaxation time $T_2$ is proportional to the width of the absorption peak at the resonance frequency. Yafet [32] showed that in metals $T_2$ is equal to the longitudinal spin relaxation time $T_1$ ($T_1 = \tau_{sf}$). In weak localization and superconducting tunneling experiments the spin orbit scattering time $\tau_{s.o.}$ is determined, with $\tau_{s.o.}$ being defined similarly in both experiments [33]. Spin orbit interaction in weak localization experiments is responsible for destructive interference when electrons are scattered at (nonmagnetic) impurities [30], whereas in the superconducting tunneling experiments it mixes up the spin-up and spin-down quasi-particle density of states [31, 34].

### 5.5.1 Quantative analysis of the spin relaxation time $\tau_{sf}$ in Cu and Al

Comparing the conductivities and spin relaxation lengths at RT and $T = 4.2$ K to each other, the impurity and phonon scattering rate and their associated spin relaxation rates can be obtained. Therefore an impurity spin relaxation ratio $a^{imp} = \tau^{imp}/\tau_{sf}^{imp}$ and an inelastic (phonon) scattering ratio $a^{ph} = \tau^{ph}/\tau_{sf}^{ph}$ can be defined. Here $(\tau^{imp})^{-1}$ and $(\tau^{ph})^{-1}$ are the impurity and phonon scattering rate and $(\tau_{sf}^{imp})^{-1}$ and $(\tau_{sf}^{ph})^{-1}$ are the impurity and phonon induced spin relaxation rate. From the measured conductivity at $T = 4.2$ K and Eq. 2.8 $\tau^{imp}$ is determined. Subsequently using the Mathiessen rule $(\tau_e)^{-1} = (\tau^{imp})^{-1} + (\tau^{ph})^{-1}$ and the RT conductivity, $\tau^{ph}$ can be determined. Note that the impurity scattering in the transparent F/N/F samples is dominated by surface scattering, as the mean free paths ($l_e \approx 60$ nm) for both the Al and Cu thin films at $T = 4.2$ K are larger than their film thicknesses (50 nm). In the calculation for Cu the free electron values [35] $N(E_F)_{Cu} = 1.8 \cdot 10^{28}$ states/eV/$m^3$ and $v_F(Cu) = 1.57 \cdot 10^6$ $m/s$ are used, whereas for Al values of $N(E_F)_{Al} = 2.4 \cdot 10^{28}$ states/eV/$m^3$ and $v_F(Al) = 1.55 \cdot 10^6$ $m/s$ are taken from Ref. [36].

Aluminum (Al)

| | $\tau_{sf}^{imp}$ $[ps]$ | $a_{imp}$ | $\tau_{sf}^{ph}$ $[ps]$ | $a_{ph}$ | Ref. |
|---|---|---|---|---|---|
| Theory | - | - | 90 [1] | $1.2 \cdot 10^{-4}$ [1] | [37] |
| Spin Injection | 100 | $0.6 \cdot 10^{-4}$ | 85 [1] | $1.1 \cdot 10^{-4}$ [1] | [18] |
| Spin Injection | 70 | $3.7 \cdot 10^{-4}$ | 124 [1] | $1.3 \cdot 10^{-4}$ [1] | [38] |
| Spin Injection | $9 \cdot 10^{3}$ | $15 \cdot 10^{-4}$ | $4 \cdot 10^{3}$ [2] | $4.8 \cdot 10^{-4}$ [2] | [39] |
| CESR | $3 - 9 \cdot 10^{3}$ | $9.0 \cdot 10^{-4}$ | $1 - 57 \cdot 10^{3}$ [3] | $2.6 \cdot 10^{-4}$ [3] | [37, 40, 41] |
| Anti-weak localiz. | 4-46 | $(0.2 - 1.2) \cdot 10^{-4}$ | - | - | [42, 43] |
| Superconducting tunn. | 8-160 | $(0.1 - 5) \cdot 10^{-4}$ | - | - | [31, 44–46] |

Copper (Cu)

| | | | | | |
|---|---|---|---|---|---|
| Spin Injection | 41 | $0.7 \cdot 10^{-3}$ | 14 [1] | $2.0 \cdot 10^{-3}$ [1] | [47] |
| CESR | $2 - 9 \cdot 10^{3}$ | $0.8 \cdot 10^{-3}$ | $2 - 21 \cdot 10^{3}$ [4] | $1.1 \cdot 10^{-3}$ [4] | [40, 48] |
| GMR | 4 | $19 \cdot 10^{-3}$ | - | - | [4] |
| Anti-weak localiz. | 5 | $1.3 \cdot 10^{-3}$ | - | - | [42, 43] |
| Energy-level spectrosc. | 20-80 | - | - | - | [49] |

[1] For T=293 K

[2] For T=45 K

[3] For a temperature range T=[1..90] K

[4] For a temperature range T=[1..60] K

Table 5.1: *Comparison of spin relaxation times of Al and Cu.* $\tau_{sf}^{imp}$ $[ps]$ *is the impurity induced spin relaxation time at low temperatures* $T \leq 4.2$ *K due to surface scattering, dislocations or grain boundaries.* $\tau_{sf}^{ph}$ $[ps]$ *is the phonon induced spin relaxation time at elevated temperatures due to inelastic phonon scattering. For definition of* $a_{imp}$ *and* $a_{ph}$ *see text.*

The obtained parameters for Cu and Al ($\tau_{sf}^{imp}$,$\tau_{sf}^{ph}$, $a^{imp}$, $a^{ph}$) are tabulated in table 5.1. From tabel 5.1 one can see that $\tau_{sf}^{ph}$ and $a_{ph}$ for Al at RT are in good agreement with the theoretical values as predicted in the ab initio bandstructure calculation by Fabian and Das Sarma [37]. They are also in agreement with the results obtained from CESR experiments and the earlier JS spin injection experiments at temperatures below 90 K. Note that the spin relaxation times are 2 orders of magnitude larger in those earlier experiments due the use of extremely clean samples with electron mean free paths of a few tens of micrometers. For Cu one can see that $\tau_{sf}^{ph}$ and $a_{ph}$ at RT are in good agreement with the results obtained from CESR

experiments at temperatures below 60 K.

The impurity scattering ratio $a^{imp}$ shows a much bigger spread in values for both Al and Cu. The different origin of the impurities in the samples used for the various measurement techniques is speculated to be the reason for this spread. For the CESR experiments the impurity scattering is caused by dislocations, whereas for our experiment it is mainly due to surface scattering.

The fact that about half of the momentum scattering processes in these Al and Cu thin films at RT is due to phonon scattering implies that the present obtained results on the spin relaxation lengths in Al and Cu can be maximally improved by a factor of about 2 at RT. This is illustrated by calculating the phonon induced spin relaxation length ($\lambda_N^{ph}$) at RT, as is shown table 5.2. $\lambda_N^{ph}$ is the maximum obtainable spin relaxation length in Al and Cu at RT, limited by the phonon induced spin flip scattering in the absence of impurity scattering: $\lambda_N^{ph} = v_F \tau^{ph} \sqrt{\frac{1}{3a_{ph}}}$.

Spin relaxation length at RT

| | $\sigma_{4.2K}$ $[\Omega^{-1}m^{-1}]$ | $\sigma_{RT}$ $[\Omega^{-1}m^{-1}]$ | $\tau^{ph}$ $[s]$ | $\lambda_N$ $[nm]$ | $\lambda_N^{ph}$ $[nm]$ [5] |
|---|---|---|---|---|---|
| Al (Ref. [18]) | $1.7 \cdot 10^7$ | $1.1 \cdot 10^7$ | $9 \cdot 10^{-15}$ | 350 | 780 [6] |
| Al (Ref. [38]) | $8 \cdot 10^7$ | $3.1 \cdot 10^7$ | $1.7 \cdot 10^{-14}$ | 600 | 1200 [6] |
| Cu (Ref. [47]) | $7.1 \cdot 10^7$ | $3.5 \cdot 10^7$ | $2.8 \cdot 10^{-14}$ | 350 | 560 [7] |

[1] $\lambda_N^{ph} = v_F \tau^{ph} \sqrt{\frac{1}{3a_{ph}}}$
[2] $v_F(Al) = 1.55 \cdot 10^6\ m/s$ [35]
[3] $v_F(Cu) = 1.57 \cdot 10^6\ m/s$ [36]

Table 5.2: *Spin relaxation lengths $\lambda_N$ and $\lambda_N^{ph}$ in Cu and Al at RT. $\lambda_N$ is the experimentally obtained spin relaxation length, whereas $\lambda_N^{ph}$ is the calculated phonon induced spin relaxation length at RT, see text. $\sigma_{4.2K}$ and $\sigma_{RT}$ are the conductivities of the Al and Cu thin films at $T = 4.2$ K and RT respectively. $\tau^{ph}$ is the phonon scattering rate at RT*

Note that for the used thin films in this thesis it is not possible to realize mean free paths of the order of micrometers as they will always be limited by surface scattering. The CESR technique is not sensitive enough to determine $\tau_{sf}^{ph}$ in these films as its resolution does not go beyond typically 1 ns. Obviously the SQUID detection technique used in Ref. [39] does not operate at RT. Therefore spin injection into thin films is rather complemen-

tary to the CESR techniques and the JS spin injection experiments in the determining $\tau_{sf}^{ph}$ in the temperature range from liquid Helium to RT, see also Fig. 2.9.

### 5.5.2 Spin injection efficiency of Py, Co and Ni ferromagnets

In addition to the spin-orbit spin scattering in metallic ferromagnets, as described above for nonmagnetic metals, there is spin flip scattering by magnons [50]. In cobalt magnons are nearly absent at low temperatures and only start to compete with the spin orbit spin flip scattering at temperatures higher than $T = 100$ K [23, 24]. The spin flip scattering by magnons has two effects. It will simply add to the spin orbit spin flip scattering rate which reduces the spin relaxation length $\lambda_F$ of the ferromagnetic metal at higher temperatures. Secondly, it will lower the bulk current polarization of the ferromagnetic metal $\alpha_F$ by changing $\sigma_\uparrow$ and $\sigma_\downarrow$ and in addition by giving rise to a "spin mixing rate" which equalizes the spin-up and spin-down currents in the ferromagnetic metal [50, 51]. The presence of spin flip scattering by magnons can therefore lower $\alpha_F$ as well as $\lambda_F$ at RT.

At low temperatures ($T < 100K$) and in absence of magnetic impurities an upper estimate can be given for the expected spin relaxation length in Co and Ni due to the spin orbit spin flip scattering only: $\lambda_F = v_F\tau_e\sqrt{\frac{1}{3a}}$, where $a$ is taken from spin flip scattering cross-sections determined by CESR experiments [15, 52] and recently from magneto-optic experiments [53]: $a_{Fe} = 1.1 \cdot 10^{-2}$, $a_{Ni} = 1.5 \cdot 10^{-2}$ and $a_{Co} = 4.2 \cdot 10^{-2}$. Using a free electron model, the spin relaxation length $\lambda_{Py}$ for Py with $\sigma_{Py} = 8.1 \cdot 10^6\ \Omega^{-1}m^{-1}$ and $\lambda_{Co}$ for Co with $\sigma_{Co} = 1.7 \cdot 10^7\ \Omega^{-1}m^{-1}$ have been estimated in this way in Ref. [5]: $\lambda_{Py}(calc) \approx 9$ nm and $\lambda_{Co}(calc) \approx 36$ nm at $T = 4.2$ K [5]. Note that $\lambda_F$ scales linearly with $\tau_e$ and thus the conductivity of the ferromagnetic metal. In this respect the reported value of $\lambda_{Co} = 59$ nm in Ref. [23, 24] is quite remarkable, because the conductivity of the Co metal ($\sigma_{co} = 6.4 \cdot 10^6$) used in Ref. [23, 24] is about 3 times smaller then used to calculate $\lambda_{Co}(calc)$ in Ref. [5] ($\sigma_{co} = 1.7 \cdot 10^7$), which makes the expected $\lambda_{Co}(calc) = 13$ nm in the experiment of Refs. [23, 24].

For Ni we derive an estimate of $\lambda_F$ using a free electron density of $5.4 \cdot 10^{28}\ m^{-3}$. With $\sigma_{Ni} = 1.6 \cdot 10^7\ \Omega^{-1}m^{-1}$ and $a_{Ni} = 1.5 \cdot 10^{-2}$, $\lambda_F$ in Ni at $T = 4.2$ K is calculated to be: $\lambda_{Ni}(calc) = 15$ nm.

Because $M > 10$ ($M = (\sigma_F\lambda_N/\sigma_N\lambda_F)(1-\alpha_F^2)$) for all our spin valve samples, $\alpha_F$ and $\lambda_F$ cannot separately be determined from the magnitude of the spin valve signal $\Delta R$. In table 5.3 therefore the "spin injection efficiency" $\alpha_F\lambda_F$ is given together with reported values from GMR experiments. Note that the thin film conductivities for Py, Co and Ni are within a factor 2 of the reported values in the GMR experiments.

| | $Ni_{80}Fe_{20}$ | | Co | | Ni | |
|---|---|---|---|---|---|---|
| | 4.2 K | RT | 4.2 K | RT | 4.2 K | RT |
| $\alpha_F\lambda_F$(nm) MSV | 1.2 | 0.5 | 0.7 | 0.3 | $< 0.1$ | $< 0.1$ |
| $\alpha_F\lambda_F$(nm) GMR | 3.6 - 4.0[1] | - | 4.5 - 27.7[2] | 8.1 - 15.5[2] | 3[3] | - |

[1] From Refs.[5–7]

[2] From Refs.[19, 21–26]

[3] From Refs.[15, 27] ($\alpha_{Ni} = 0.2$) and using $\lambda_{Ni}(calc) = 15$ nm

Table 5.3: *Spin injection efficiencies $\alpha_F\lambda_F$ in nm for three different ferromagnetic metals. The data is deduced from the mesoscopic spin valve (MSV) experiments with transparent contacts in a non local geometry using Cu as nonmagnetic metal and compared with results from GMR experiments.*

Table 5.3 shows that the obtained spin injection efficiency of the Py ferromagnet $\alpha_{Py}\lambda_{Py}$ is in quantative agreement with the values reported in GMR experiments ($\alpha_{Py} = 0.7$, $\lambda_{Py} = 5\ nm$), taking into account that the obtained $\alpha_{Py}\lambda_{Py}$ represents a minimal value due to a partially shunting of the injected current by the Cu wire on top of the Py electrodes. The reduction of $\alpha_{Py}\lambda_{Py}$ at RT beyond the ratio 1.8 of the Py conductivies at $T = 4.2$ K and RT could be attributed to magnons, lowering $\alpha_F$ at RT.

For the Co and the Ni ferromagnets much smaller spin injection efficiencies $\alpha_F\lambda_F$ are observed, being more than 1 order of magnitude smaller than values of $\alpha_F\lambda_F$ obtained in GMR experiments. So the question is, what is causing this rather large reduction of the spin valve signal?

First the possible influences of an existing interface resistance at the Co/Cu and Ni/Cu interfaces are discussed. From the resistance measured in a conventional geometry an upper estimate of the (diffusive) interface resistances can be determined. For the Co/Cu/Co spin valve of Fig. 5.7 an upper limit for a single Co/Cu interface is found to be $R_{int} = 0.4\ \Omega$, whereas for the Ni/Cu/Ni spin valve of Fig. 5.8 $R_{int} = 0.6\ \Omega$ is found. Comparing the associated interface resistivity ($\approx 5 \cdot 10^{-15}\ \Omega m^2$) with calculated values [20, 54–57] and values obtained from GMR [9, 22], the observed interface resistivity is about 5 times larger than expected for Co/Cu (specular or diffusive) interfaces. In case these Co/Cu and Ni/Cu interface resistances are spin dependent, the spin signal would be (largely) increased as the sign of the bulk and interface spin asymmetries of Co, Ni and Cu are found both to be positive [15, 55–58] ($\alpha_F > 0$ and $\gamma > 0$). However this is clearly not observed.

In the case of spin independent interface resistances, the interface resistance for each spin channel ($\approx 1\ \Omega$) will not reduce the measured spin valve signal much as the spin independent interface resistance just adds to the

(larger) spin independent resistance of the Cu strip of about 6 Ω for both the spin-up and spin-down channels (see Sec. 5.2.4, Eqs. 5.5 and 5.6).

The spin signal can therefore only be significantly be reduced due to a possible spin flip scattering mechanism at the interface, an effect which has recently been studied in CPP-GMR spin valves [59, 60]. The physical origin of this mechanism could be diverse, for instance: surface roughness creating local magnetic fields due to the formation of random domains or the formation of anti-ferromagnetic oxides CoO and NiO at the surface during the time in between the Kaufmann sputtering and the Cu deposition. However the interfacial structure of the devices is basically unknown and the most probable cause cannot be analyzed. If however such mechanisms would exist at the Co/Cu and Ni/Cu interface, they probably would also appear at the Py/Cu interface. The Py/Cu/Py spin valve data show that their manifestation in these samples is apparently absent or less severe.

Secondly, a change in the bulk properties of the Co and Ni could explain the small spin valve signals, i.e. a (substantial) shortening of the bulk spin relaxation length or a reduction of the polarization $\alpha_F$ in the Co and Ni ferromagnetic metals. In CIP-GMR experiments [61] a strong decrease of more than an order of magnitude in the GMR signal was reported upon changing the base ($H_2O$) pressure of the sputter deposition chamber from $10^{-8}$ to $10^{-5}$ mbar, just before deposition the Co and Cu layers. This decrease in GMR signal was more than could be accounted for by the increase in resistivity of the layers. In the deposition chamber at Groningen the base pressure is only $10^{-7}$ mbar, whereas in the experiments e.g. on Co/Ag multilayers [22] the base pressure is of the system is $10^{-8}$ mbar. However, theoretical work [58] does predict a bulk current polarization $\alpha_{Co} \approx 0.6$ for fcc-Co, having a conductivity close to our thin Co films $\sigma_{Co} = 7.3 \cdot 10^6\ \Omega^{-1}m^{-1}$. Unfortunately the crystallinity and/or the crystal orientation of the Co films used in this thesis are unknown. Note that the Co layers in the Co/Cu multilayered nanowires [23, 24] and the Co/Ag multilayers [22] have a hcp structure.

Finally, it cannot be excluded that the deviation from a true perpendicular current injection (see Fig. 2.2) in our planar device geometry could influence the magnitude of the spin valve signal. For ballistic transport in Co/Cu multilayers the magnetoresistance (MR) ratio was (theoretically) shown to decrease by a factor of 10 for shallow injection angles with the multilayer plane [56].

## 5.6 Conclusions

Spin injection and accumulation in metallic mesoscopic spin valves with transparent contacts is demonstrated. It is shown that in a conventional measurement geometry the magnetoresistance effects of the injecting and detecting contacts can be much larger than the spin valve effect, making it impossible to observe the spin valve effect in a 'conventional' measurement geometry. However, these contact effects can be used to monitor the magnetization reversal process of the spin injecting and detecting contacts, see Chapter four. In a non-local measurement geometry the spin valve effect can be completely isolated. Using this geometry spin relaxation lengths in Cu are found to be around 1 $\mu m$ at $T =$ 4.2 K and 350 nm at RT and spin relaxation lengths in Al are found to be around 1.2 $\mu m$ at $T =$ 4.2 K and 600 nm at RT. The associated spin relaxation times in Al and Cu are in good agreement with theory and values from experiments previously reported in the literature. A rather striking result is that the spin relaxation lengths in Al and Cu at RT are fundamentally limited by phonon scattering to a maximum length of about 1.2 $\mu m$ and 600 nm for Al and Cu respectively. For the Py material spin relaxation lengths and current polarizations are found to be in agreement with GMR experiments. However for Co values of $\alpha_F \lambda_F$ are obtained which are up to a factor 40 smaller than their GMR counterpart. For Ni electrodes the spin valve measurement were unsuccessful, no spin valve signal could be resolved within the limits of our experimental accuracy, corresponding with $\alpha_F \lambda_F$ at least a factor 10 lower than expected. Three possible reasons could be identified causing the low polarization and/or spin relaxation lengths, however the exact origin of the reduction is unclear.

## References

[1] F. G. Monzon and M. L. Roukes, J. Magn. Magn. Mater. **198**, 632 (1999).

[2] J. Nitta, T. Schäpers, H. B. Heersche, T. Koga, Y. Sato, and H. Takayanagi, Jap. J. Appl. Phys. **41**, 2497 (2002).

[3] F. J. Jedema, M. S. Nijboer, A. T. Filip, and B. J. van Wees, Journal of Superconductivity **15 (1)**, 27 (2002).

[4] Q. Yang, P. Holody, S.-F. Lee, L. L. Henry, R. Loloee, P. A. Schroeder, W. P. Pratt, Jr., and J. Bass, Phys. Rev. Lett. **72**, 3274 (1994).

[5] S. Dubois, L. Piraux, J. George, K. Ounadjela, J. Duvail, and A. Fert, Phys. Rev. B **60**, 477 (1999).

[6] S. D. Steenwyk, S. Y. Hsu, R. Loloee, J. Bass, and W. P. Pratt Jr., J. Mag. Magn. Mater. **170**, L1 (1997).

[7] P. Holody, W. C. Chiang, R. Loloee, J. Bass, W. P. Pratt, Jr., and P. A. Schroeder, Phys. Rev. B **58**, 12230 (1998).

[8] S. F. Lee, W. P. Pratt, Jr., R. Loloee, P. A. Schroeder, and J. Bass, Phys. Rev. B **46**, 548 (1992).

[9] Q. Yang, P. Holody, R. Loloee, L. L. Henry, W. P. Pratt, Jr., P. A. Schroeder, and J. Bass, Phys. Rev. B **51**, 3226 (1995).

[10] M. Johnson, Science **260**, 320 (1993).

[11] M. Johnson, Phys. Rev. Lett. **70**, 2142 (1993).

[12] M. Johnson, J. Appl. Phys. **75**, 6714 (1994).

[13] M. Johnson, Nature **416**, 809 (2002).

[14] M. Johnson, Semicond. Sci. Technol. **17**, 298 (2002).

[15] C. Vouille, A. Barthélémy, F. E. Mpondo, A. Fert, P. A. Schroeder, S. Y. Hsu, A. Reilly, and R. Loloee, Phys. Rev. B **60**, 6710 (1999).

[16] A. Fert and S. Lee, Phys. Rev. B **53**, 6554 (1996).

[17] S. Hershfield and L. Z. Zhao, Phys. Rev. B **56**, 3296 (1997).

[18] F. J. Jedema, H. B. Heersche, A. T. Filip, J. J. A. Baselmans, and B. J. van Wees, Nature **416**, 713 (2002).

[19] J.-P. Ansermet, J. Phys.:Condens. Matter **10**, 6027 (1998).

[20] M. A. M. Gijs and G. E. W. Bauer, Advances in Physics **46**, 285 (1997).

[21] J. Bass and W. P. Pratt Jr., J. Mag. Magn. Mater. **200**, 274 (1999).

[22] S.-F. Lee, Q. Yang, P. Holody, R. Loloee, J. H. Hetherington, S. Mahmood, B. Ikegami, K. Vigen, L. L. Henry, P. A. Schoeder, et al., Phys. Rev. B **52**, 15426 (1995).

[23] L. Piraux, S. Dubois, C. Marchal, J. Beuken, L. Filipozzi, J. F. Despres, K. Ounadjela, and A. Fert, J. Mag. Magn. Mater. **156**, 317 (1996).

[24] L. Piraux, S. Dubois, A. Fert, and L. Beliard, Eur. Phys. J. B **4**, 413 (1998).

[25] J.-P. A. B. Doudin, A. Blondel, J. Appl. Phys. **79**, 6090 (1996).

[26] U. Ebels, A. Radulescu, Y. Henry, L. Piraux, and K. Ounadjela, Phys. Rev. Lett. **84**, 983 (2000).

[27] H. Kubota, M. Sato, and T. Miyazaki, Phys. Rev. B **52**, 343 (1995).

[28] W. P. Pratt, Jr., S.-F. Lee, J. M. Slaughter, R. Loloee, P. A. Schroeder, and J. Bass, Phys. Rev. Lett. **66**, 3060 (1991).

[29] C. Kittel, *Introduction to Solid State Physics* (Wiley 7th edition, New York, 1996).

[30] G. Bergmann, Physics Reports **107**, 1 (1984).

[31] R. Meservey and P. M. Tedrow, Physics Reports **238**, 173 (1994).

[32] Y. Yafet, *Solid State Physics* (Academic, New York, 1963).

[33] J. A. X. Alexander, P. M. Tedrow, and T. P. Orlando, Phys. Rev. B **34**, 8157 (1986).

[34] P. Fulde, Adv. Phys. **22**, 667 (1973).

[35] N. W. Ashcroft and N. D. I. Mermin, *Solid State Physics* (W.B. Saunders Company, 1976).

[36] D. A. Papaconstantopoulos, *Handbook of the band structure of elemental solids* (Plenum, New York, 1986).

[37] J. Fabian and S. D. Sarma, Phys. Rev. Lett. **83**, 1211 (1999).

[38] F. J. Jedema, M. S. Nijboer, A. T. Filip, and B. J. van Wees, submitted to Phys. Rev. B.

[39] M. Johnson and R. H. Silsbee, Phys. Rev. Lett. **55**, 1790 (1985).

[40] F. Beuneu and P. Monod, Phys. Rev. B **13**, 3424 (1976).

[41] D. Lubzens and S. Schultz, Phys. Rev. Lett. **36**, 1104 (1976).

[42] G. Bergmann, Phys. Rev. B **29**, 6114 (1984).

[43] J. M. Gordon, C. J. Lobb, and M. Tinkham, Phys. Rev. B Rap. Comm. **28**, 4046 (1983).

[44] R. Meservey, P. M. Tedrow, and R. C. Bruno, Phys. Rev. B **11**, 4224 (1975).

[45] C. Grimaldi and P. Fulde, Phys. Rev. Lett. **77**, 2550 (1996).

[46] D. J. Monsma and S. S. P. Parkin, Appl. Phys. Lett. **77**, 720 (2000).

[47] F. J. Jedema, A. T. Filip, and B. J. van Wees, Nature **410**, 345 (2001).

[48] S. Schultz and C. Latham, Phys. Rev. Lett. **15**, 148 (1965).

[49] J. R. Petta and D. C. Ralph, Phys. Rev. Lett. **2001**, 266801 (87).

[50] A. Fert, J. L. Duvail, and T. Valet, Phys. Rev. B **52**, 6513 (1995).

[51] A. Fert and I. A. Campbell, J. Phys. F **6**, 849 (1976).

[52] P. Monod and S. Schultz, J. Physique **43**, 393 (1982).

[53] B. Koopmans, M. van Kampen, J. T. Kohlhepp, and W. J. M. de Jonge, Phys. Rev. Lett. **85**, 844 (2000).

[54] P. M. Levy, Solid State Phys. **47**, 367 (1994).

[55] K. M. Schep, J. B. A. N. van Hoof, P. J. Kelly, G. E. W. Bauer, and J. E. Inglesfield, Phys. rev. B **56**, 10805 (1997).

[56] K. M. Schep, Ph.D. thesis, Delft University of Technology (1997).

[57] K. Xia, P. J. Kelly, G. E. W. Bauer, I. Turek, J. Kudrnovsky, and V. Drchal, Phys. Rev. B **63**, 064407 (2001).

[58] E. Y. Tsymbal and D. Pettifor, Phys. Rev. B **54**, 15314 (1996).

[59] W. Park, D. V. Baxter, S. Steenwyk, I. Moraru, W. Pratt, Jr., and J. Bass, Phys. Rev. B **62**, 1178 (2000).

[60] C. H. Marrows and B. Hickey, Phys. Rev. B **63**, 220405 (2001).

[61] W. F. Egelhoff, Jr., P. J. Chen, C. J. Powell, M. Stiles, R. D. McMichael, C.-L. Lin, J. M. Sivertsen, J. H. Judy, K. Takano, et al., J. Appl. Phys. **79**, 5277 (1996).